Electronic Supplementary material

Ultrafast electron dynamics in excited states of conjugated thiophene-fluorene organic polymer (pF8T2) thin films

T. Reiker,[a,b] Z. Liu,[c] C. Winter,[b] M.V. Cappellari,[d] D. Gonzalez Abradelo,[d] C. A. Strassert,[d] D. Zhang,[c] H. Zacharias[a,b]

[a] Center for Soft Nanoscience, University of Münster, 48149 Münster, Germany

[b] Physics Institute, University of Münster, 48149 Münster, Germany

[c] Organic Solids Laboratory, Institute of Chemistry, Chinese Academy of Science, Beijing 100190, P.R. of China

[d] Center for Nanotechnology and Institute for Inorganic and Analytical Chemistry, University of Münster, Heisenbergstraße 11, 48149 Münster, Germany

Cross correlation of the laser pulses of λ_{pump} = 460 nm and λ_{probe} = 257 nm

In order to evaluate the time-dependent electron dynamics we determined the cross correlation width and the temporal zero point within the measurements by recording the two-photon photoelectron signal from a H-terminated silicon wafer without any polymer adsorbed. Only the part of the spectrum that we assign to the hot electrons was used. This corresponds to the signal of electrons at the highest kinetic energy of E_{kin} ~ 2 eV. Accordingly, the excitation and the transition into the vacuum occurred via a virtual state. Therefore, we consider this process of excitation and decay to be instantaneous within the measurement resolution. The time-dependent signal in Figure S1 corresponds to the cross correlation of the pump of λ_{pump} = 460 nm and probe λ_{probe} = 257 nm pulses. A Gaussian fit yields a cross correlation width of τ_{FWHM} = (68 ± 1) fs.

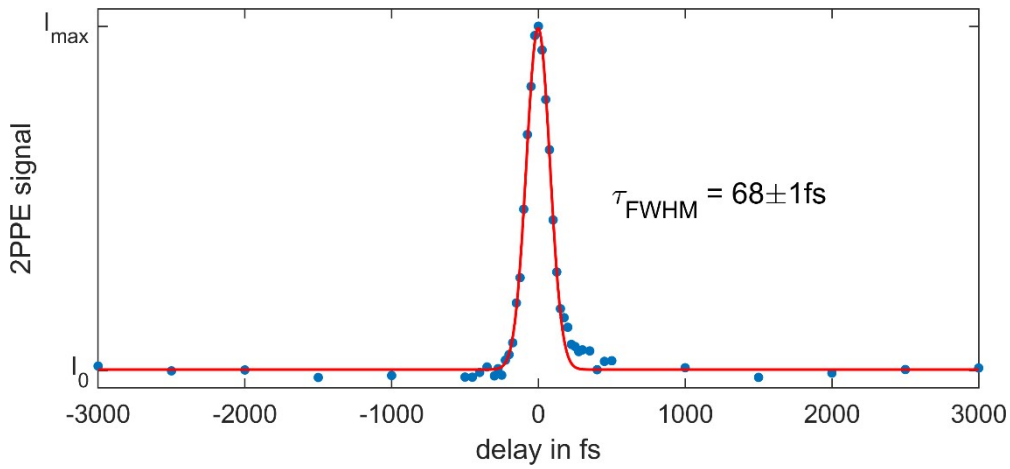

Figure S1. *Instantaneous 2PPE signal of hot electrons from a H-terminated silicon wafer. The cross-correlation width of τ_{FWHM} = (68 ± 1) fs is measured for λ_{pump} = 460 nm and λ_{probe} = 257 nm .*

Steady state emission spectra and Time Correlated single photon counting (TCSPC)

Steady-state excitation and emission spectra were measured on a FluoTime 300 spectrometer from PicoQuant equipped with a 300 W ozone-free Xe lamp (250-900 nm), a 10 W Xe flashlamp (250-900 nm, pulse width ca. 1 µs) with repetition rates of 0.1 – 300 Hz, a double excitation monochromator (Czerny-Turner type, grating with 1200 lines/mm, blaze wavelength: 300 nm), diode lasers (pulse width < 80 ps) operated by a computer-controlled laser driver PDL-828 "Sepia II" (repetition rate up to 80 MHz, burst mode for slow and weak decays), On the emission side two double-grating monochromators (Czerny-Turner, selectable gratings blazed at 500 nm with 2.7 nm/mm dispersion and 1200 lines/mm, or blazed at 1200 nm with 5.4 nm/mm dispersion and 600 lines/mm) with adjustable slit width between 25 µm and 7 mm can be utilized. Two Glan-Thompson polarizers for excitation after the Xe-lamps and emission after the sample.

Two detectors (PMA Hybrid-07 from PicoQuant with transit time spread FWHM < 50 ps, 200 – 850 nm, or a H10330C-45-C3 NIR detector with transit time spread FWHM 0.4 ns, 950-1700 nm from Hamamatsu) can be mounted. For steady-state spectra and photoluminescence lifetimes were acquired in TCSPC mode by using a PicoHarp 300 (minimum base resolution 4 ps) or in MCS mode with a TimeHarp 260 (where up to several ms can be traced). Emission and excitation spectra were corrected for source intensity (lamp and grating) by standard correction curves.

Franck-Condon fits

The Franck-Condon overlap integral is related to the Huang-Rhys factor $S_i = \frac{M_i \omega_i}{2\hbar}(\Delta Q_i)$, with the reduced mass M_i, angular frequency ω_i, and ΔQ_i proportional to the zero-point configuration coordinate for the respective oscillator *i*.

In general, Franck-Condon fits can be used to analytically describe the absorption and emission spectra of conjugated polymers. For some simple conjugated polymers in solution, a series of Gaussian shaped transitions Γ is often used, where the spacing of these transitions is given by the vibrational energy ω_0, and the ratio of the height distribution is represented by the Huang-Rhys parameter *S*, for the m^{th} vibronic level. The absorption and emission spectra, where $n(\hbar\omega)$ is the refractive index, can be modelled as[1,2]:

$$I_{Abs}(\hbar\omega) \propto [n(\hbar\omega)\cdot\hbar\omega]\cdot\sum_{m\geq 0}\frac{S^m e^{-S}}{m!}\cdot\Gamma\big(\hbar\omega-(\hbar\omega_0+m\hbar\omega_p)\big) \qquad (1)$$

$$I_{PL}(\hbar\omega) \propto [n(\hbar\omega)\cdot\hbar\omega]^3\cdot\sum_{m\geq 0}\frac{S^m e^{-S}}{m!}\cdot\Gamma\big(\hbar\omega-(\hbar\omega_0-m\hbar\omega_p)\big) \qquad (2)$$

However, even for simple conjugated polymers of the first generation the description is more complex. Combinations of several intramolecular vibrational modes can occur[2]:

$$I_{Abs}(\hbar\omega) = [n(\hbar\omega)\cdot\hbar\omega]\cdot\sum_{m_i}\prod_i\frac{S_i^{m_i}}{m_i!}e^{-S_i}\cdot\Gamma\cdot\delta\left(\hbar\omega-\left(\hbar\omega_0+\sum_i m_i\hbar\omega_{m_i}\right)\right) \qquad (3)$$

$$I_{PL}(\hbar\omega) = [n(\hbar\omega)\cdot\hbar\omega]^3 \cdot \sum_{m_i}\prod_i \frac{S_i^{m_i}}{m_i!}e^{-S_i}\cdot\Gamma\cdot\delta\left(\hbar\omega-\left(\hbar\omega_0+\sum_i m_i\hbar\omega_{m_i}\right)\right) \quad (4)$$

In thin films, different phases or aggregates can contribute to the respective spectrum. The exciton coupling parameter J quantitatively describes the interaction between individual polymer strands and aggregates and is given, e.g., for P3HT, by the ratio of the first and second absorption peaks.[3,4]

$$\frac{A_{0-0}}{A_{0-1}} = \frac{n_{0-0}}{n_{0-1}S}\frac{\left(1-\frac{J}{\omega_0}e^{-S}\sum_{n>0}\frac{S^n}{n!n}\right)^2}{\left(1-\frac{J}{\omega_0}e^{-S}\sum_{n\neq 1}\frac{S^n}{n!(n-1)}\right)^2} \quad (5)$$

According to Scharsich et al.,[4] in this case the Huang-Rhys factor *S* can be determined by the photoluminescence of a single emitter. Furthermore, it is not necessary to consider all vibrations but to generalize to a single effective vibrational energy ω_0.[4] The complete spectra can then be described by[5,6]:

$$I_{PL}(\hbar\omega) = [n(\hbar\omega)\cdot\hbar\omega]^3\cdot\left[\alpha\cdot\exp\left[-\frac{(\hbar\omega-\hbar\omega_0)^2}{2\sigma}\right]+\sum_{m=1}\frac{S^m}{m!}e^{-S}\cdot\exp\left[-\frac{(\hbar\omega-\hbar\omega_0-m\hbar\omega_p)^2}{2\sigma}\right]\right] \quad (6)$$

,

where α is a constant associated with disorder and spatial correlation length. For the absorption in thin films the free exciton bandwidth W=|4J| becomes significant[7]:

$$I_{Abs}(\hbar\omega) = [n(\hbar\omega)\cdot\hbar\omega]\sum_{m=0}\frac{e^{-S}S^m}{m!}\left(1-\frac{We^{-S}}{2\hbar\omega_p}\left(\sum_{n\neq m}\frac{S^n}{n!(n-m)}\right)\right)^2\cdot\exp\left[-\frac{(\hbar\omega-\hbar\omega_0-m\hbar\omega_p)^2}{2\sigma}\right] \quad (7)$$

.

Often the assumption $S = 1$ is used, assuming that *S* does not change during aggregation, which assumes a weak coupling. Spano introduced the weakly coupled H/J aggregate model, where the ratio of the lowest (0-0) to the first vibronic absorption (0-1) of either H- or J-aggregates are more prominent.[5,8,9]

$$\frac{A_{0-0}}{A_{0-1}} \approx \left(\frac{1-0.48J_{k=0}/E_p}{1+0.146J_{k=0}/E_p}\right)^2. \quad (8)$$

The energy of the coupled phonon mode is about $E_p = \hbar\omega_p$ = 0.18 eV for carbon related bonds, and the excitonic shift ($J_{k=0}$ = 2J_0, where *k* represents the wave vector of the phonon) is related to the type of aggregate: $J_{k=0} > 0$ is for H- and $J_{k=0} < 0$ for J-aggregates.[8] That leads to amplitude ratios $A_{0-0}/A_{0-1} < 1$ for H-aggregates and $A_{0-0}/A_{0-1} > 1$ for J-aggregates. With the substitution of the free exciton bandwidth $W = |4J_0| = 2|J_{k=0}|$, e.g. for P3HT[5], the intensity ratio between the first and second peak can be quantified by the free exciton bandwidth[9]:

$$\frac{A_{0-0}}{A_{0-1}} \approx \left(\frac{1-0.24W/E_p}{1+0.073W/E_p}\right)^2. \quad (9)$$

Franck-Condon fits for absorption and photoluminescence spectra

For modelling the absorption and photoluminescence spectra equation (6) and (7) where used, but for the emission spectra, a shift in *E*p and σ were allowed, as the (0-0) peak emerges with annealing. Table S1 summarizes all retrieved parameters from the fitting procedure. Figure S3 shows the measured photoluminescence and absorbance for pF8T2. Before modeling the absorbance spectra, a broad gaussian background was subtracted, see Figure S2. Differences in the vibrational modes between absorption and emission are anticipated. In absorption, electronically excited states (S_1) are analyzed, whereas in emission, de-excitation to the electronic ground state is investigated.

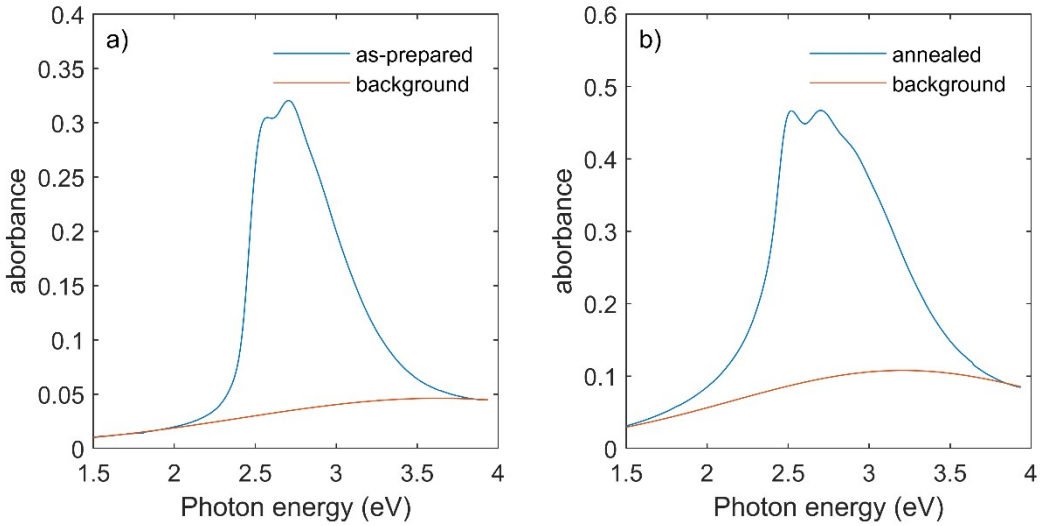

Figure S2. *Subtracted background for the Frank-Condon analysis of the absorption spectra for a) as-prepared and b) annealed sample.*

Table S1. *Fitting parameters for the Frank-Condon analysis of absorption and emission spectra*

	Quarz absorbance as-prepared	Quarz absorbance annealed	Quarz emission as-prepared	Quarz emission annealed	H-Silicon emission as-prepared	H-Silicon emission annealed
E_{00}^{O} [eV]	2.535±0.001	2.492±0.001	2.401±0.001	2.423±0.002	2.370±0.003	2.410±0.003
E_p^{O} [eV]	0.178±0.001	0.177±0.001	0.148±0.001	0.156±0.001	0.134±0.004	0.152±0.001
S_1^{O}	1.048±0.144	0.984±0.063	1.598±0.011	2.074±0.014	1.636±0.037	2.617±0.021
E_{00}^{A}[eV]	2.846±0.013	2.788±0.006				
E_p^{A} [eV]	0.182±0.007	0.178±0.002				
S_2^{A}	1.359±0.219	1.674±0.081				
α			0	0.319±0.023	0	0.693±0.045
W [eV]	-0.018±0.037	-0.050±0.019				
Ratio O/A	0.301±0.049	0.706±0.025				
Shift (0-0)				0.015±0.004		0.005±0.006

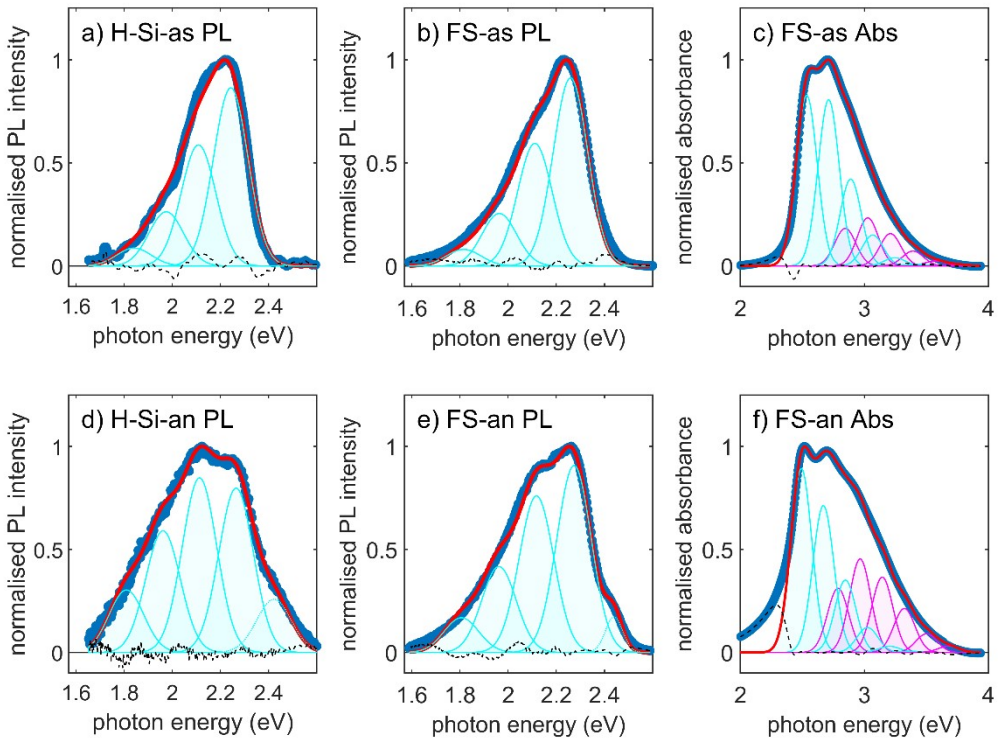

Figure S3. *Franck-Condon fits for pF8T2 as-prepared on a) H-Si, b) and c) on fused silica, as well as the annealed samples d) H-Si, e) and f) fused silica. Data points in blue, sum fit in red and dotted black the difference between signal and fit. In light blue are shown, the individual contributions of the vibronic states in the ordered phase and in pink the contributions of the amorphic phase.*

Fits for the single colour two-photon photoelectron spectroscopy

For the single-colour photoelectron spectroscopy with the NOPA the wavelength was tuned in 10 nm steps from λ = 460 to 350 nm. Each spectrum was acquired for a dwell time of t = 300 s for each step. The spectra were plotted semi-logarithmically and an exponential background was subtracted from the plot to eliminate the influence of the secondary electrons, see Figure S 4. The resulting peak structure was fitted by two Gaussians, see Figure S 5 a-g. For wavelengths shorter than λ = 400 nm, or photon energies larger than hv = 3.10 eV, two new states dominate. They appear at low kinetic energies and their centre shift to higher kinetic energies with increasing photon energy. To evaluate these states, Figure S 5 h-m, an additional exponential background was subtracted, as these overlap strongly with the secondary electrons and additional secondary electrons are generated.

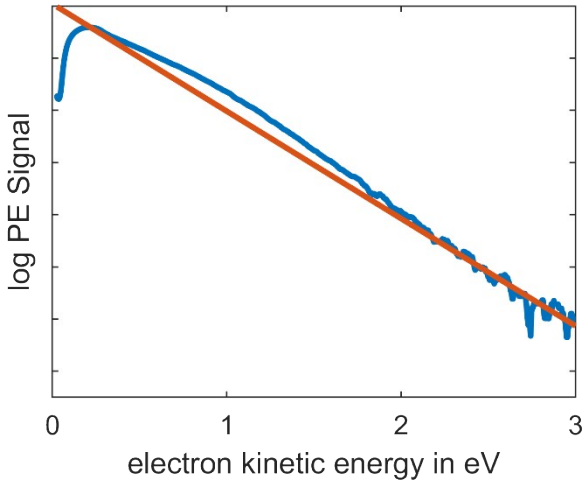

Figure S4. *Background subtraction of the static photoelectron spectra excited with the NOPA (λ = 460 nm-350 nm), exemplarily for λ = 430 nm.*

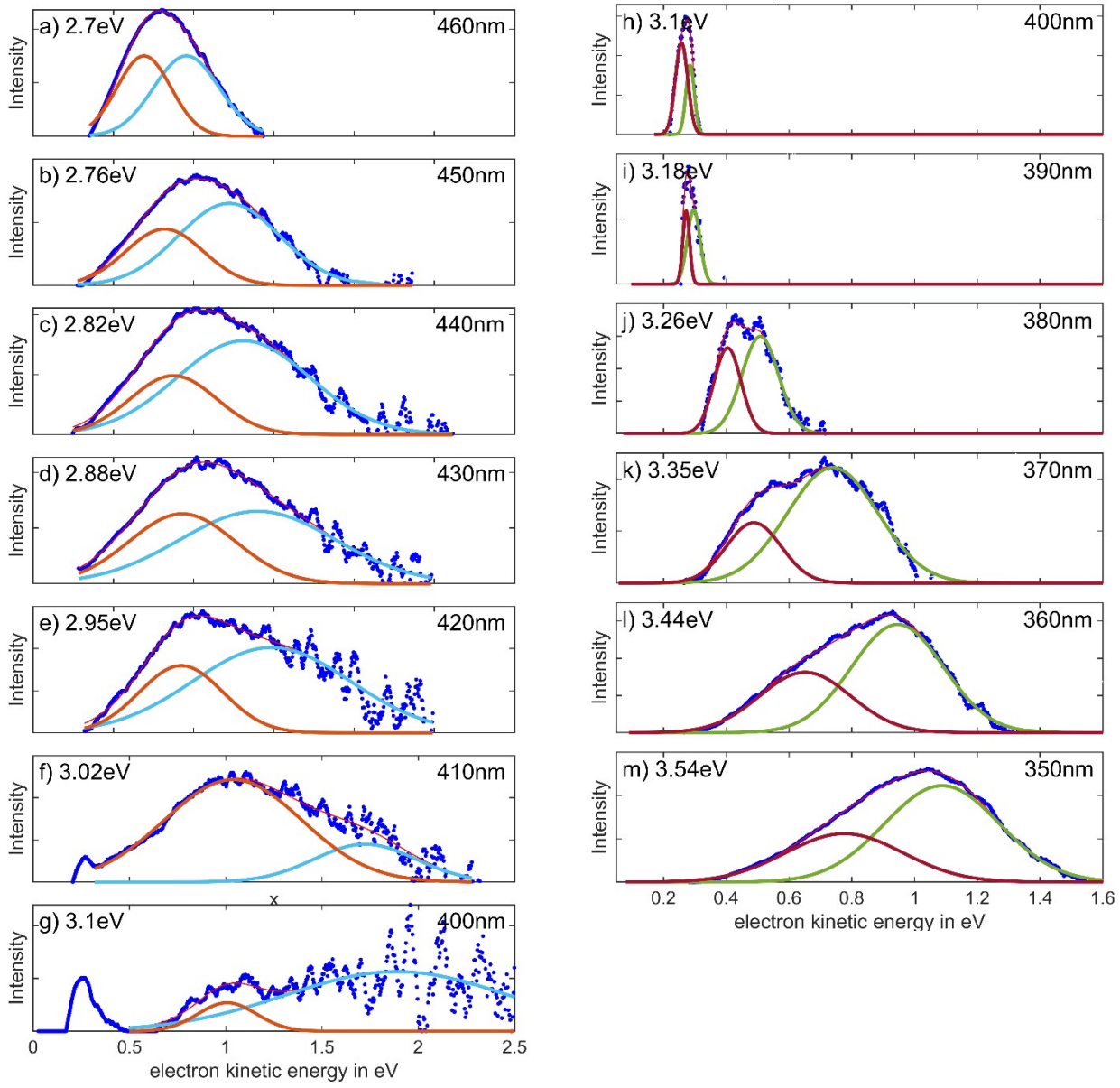

Figure S5. *Evolution of the background corrected photoelectron spectra for different two-photon excitation wavelength. In dark blue are shown the experimental data points. The experimental data are approximated by two Gaussian functions, for (a) through (g) in light blue and orange, and for (h) through (m) in green and dark red. The positions of the maxima of these fits are shown in fig.4.*

Lifetime fits for tr-2PPE measured with λ_{pump} = 460 nm and λ_{probe} = 257 nm

The spectra were binned into energy intervals of ΔE_{kin} = 100 meV. For the data points at E_{kin} = 2 eV we integrated over ΔE_{kin} = 200 meV due to a lower count rate. The background was determined from the count rates of the negative delays for each electron kinetic energy. The determined background was subtracted from the count rates for all delays using a linear function. Figure S6 shows the corresponding time-dependent signals and the corresponding fits for the respective kinetic energies. Black circles (•) represent data for as-prepared and red crosses (+) for annealed samples. The solid lines are the fourfold exponential fits to the data points. The fourth lifetime was fixed at τ_4 = 150 ps in accordance with the shortest lifetime of the TCSPC fluorescence measurements. The residuals of the fits are shown in fig. S7. They amount to less than about 1.3 % of the amplitudes of the tr-2PPE signal.

The corresponding relative amplitudes are given in Figure S 8. While A_2 and A_4 are largely independent of the kinetic energy, the relative proportions of A_1 show a rather decreasing and those of A_3 an increasing tendency from higher to lower kinetic energies. The annealing of the sample leads to an overall higher contribution of the shortest lifetime. Therefore, A_2 and A_3 are reduced accordingly.

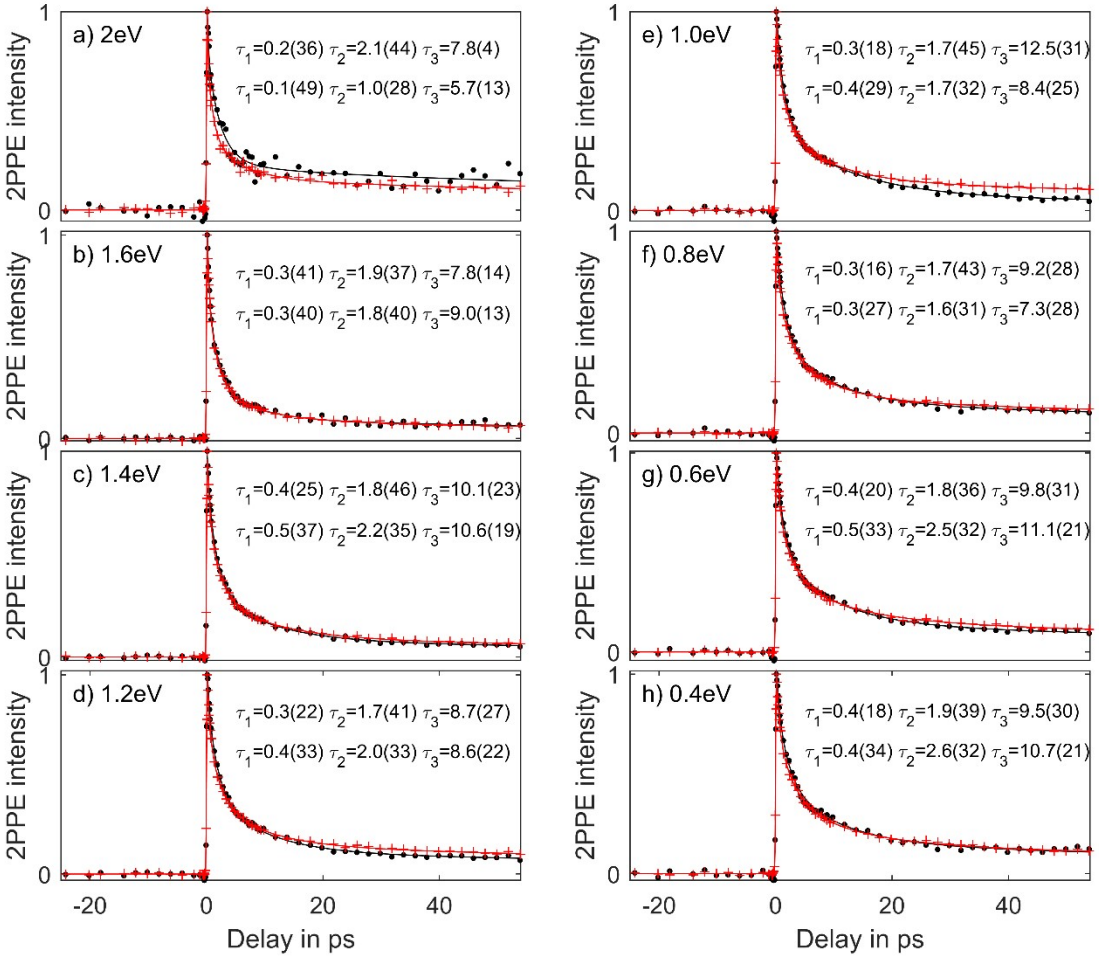

Figure S6. *Lifetime fits for tr-2PPE measured with λ_{pump} = 460 nm and λ_{probe} = 257 nm. For a) the data were integrated over ΔE_{kin} = 200 meV, for b) - h) over ΔE_{kin} = 100 meV. The values in parenthesis indicate the relative contributions (A_k%) of the respective decay to the 2PPE signal. Black circles (•) represent data for as-prepared and red crosses (+) for annealed samples.*

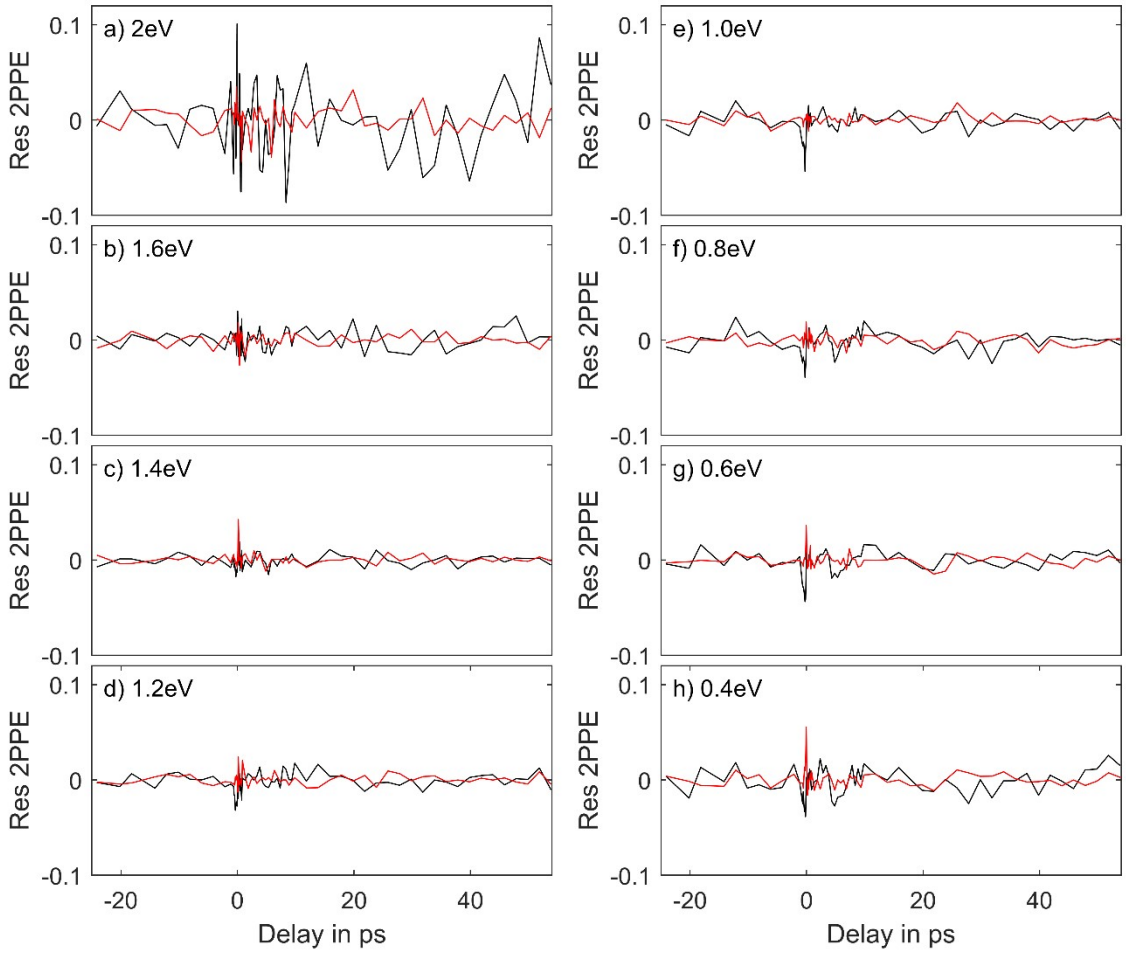

Figure S7. *Residuals for tr-2PPE fits in* Figure S6. *Black for as-prepared and red for annealed ones. The rms values for are in general below > 1.3%, for the as-prepared fit in a) at 2 eV the rms variation is about 3.8% due to low signal-to-noise ratio.*

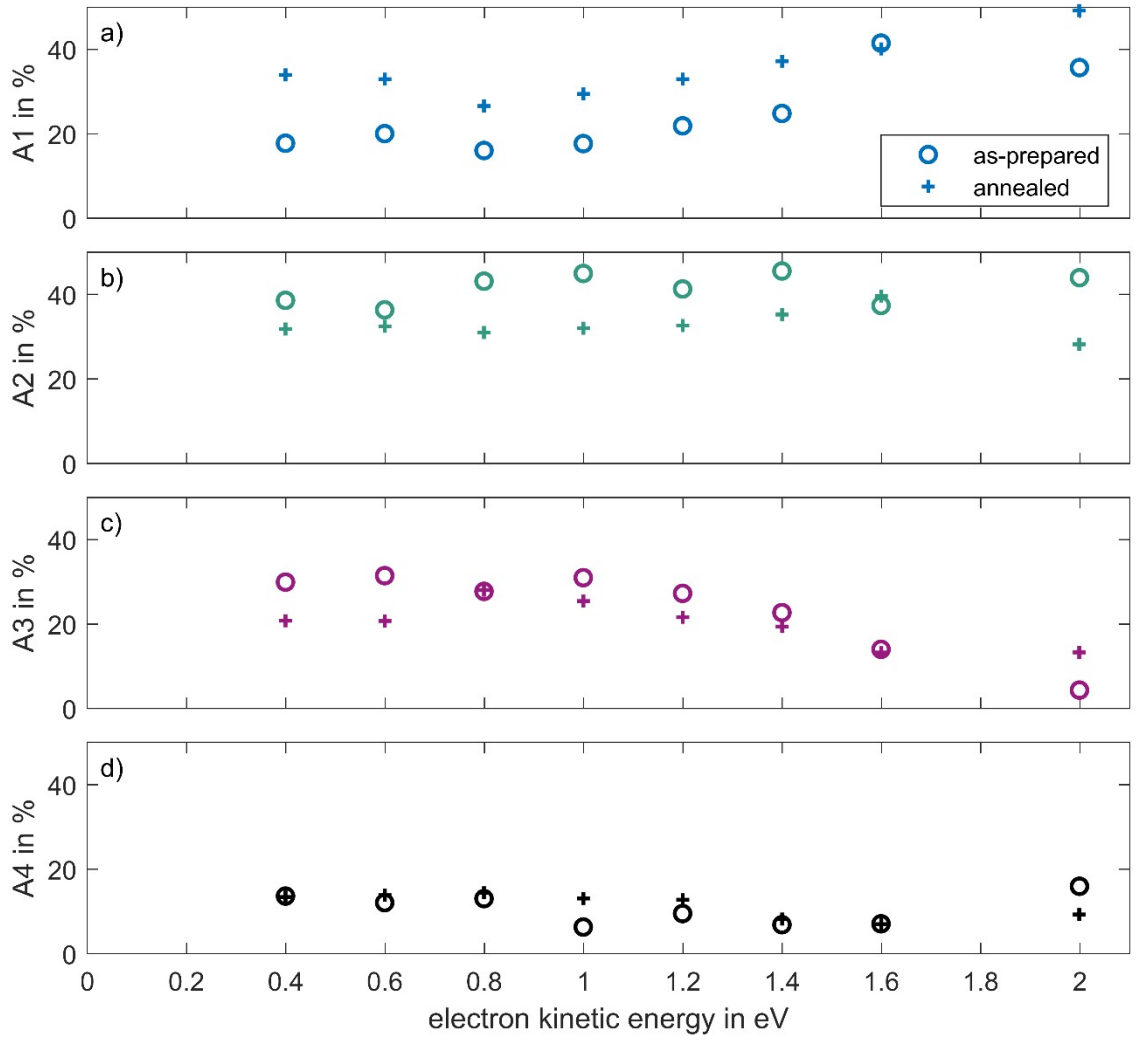

Figure S8. *Development of the weighting factors A_K of the lifetimes retrieved from tr-2PPE spectra measured with λ_{pump} = 460 nm and λ_{probe} = 257. (+) for the annealed and (o) for the as-prepared case; for A_1 in blue, A_2 in green, A_3 in purple and A_4 in black.*

Alternative fits with stretched exponential function for tr-2PPE measured with λ_{pump} = 460 nm and λ_{probe} = 257 nm

For modeling the tr-2PPE data with a stretched exponential the following fit function was used:

$$I_{2PPE} \sim A_1 \exp\left(\left(\frac{\Delta\tau - \tau_0}{\tau_1}\right)^{1/2}\right)\left(1 + \operatorname{erf}\left(\frac{\Delta\tau - \tau_0 - {\tau_p^2}/{\tau_k}}{\tau_p\sqrt{2}}\right)\right) + A_2\left(1 + \operatorname{erf}\left(\frac{\Delta\tau - \tau_0}{\tau_p\sqrt{2}}\right)\right) \quad (10)$$

Here $\tau_1$represents the decay time, $\Delta\tau$ the delay between pump and probe pulse, τ_0 a possible offset from the temporal overlap, τ_p the cross-correlation width, A_1 the amplitude of the stretched exponential decay and A_2 the amplitude of a possible background. In contrast to the multiexponential model, there is a clear disagreement between fit and experimental data, especially towards longer lifetimes.

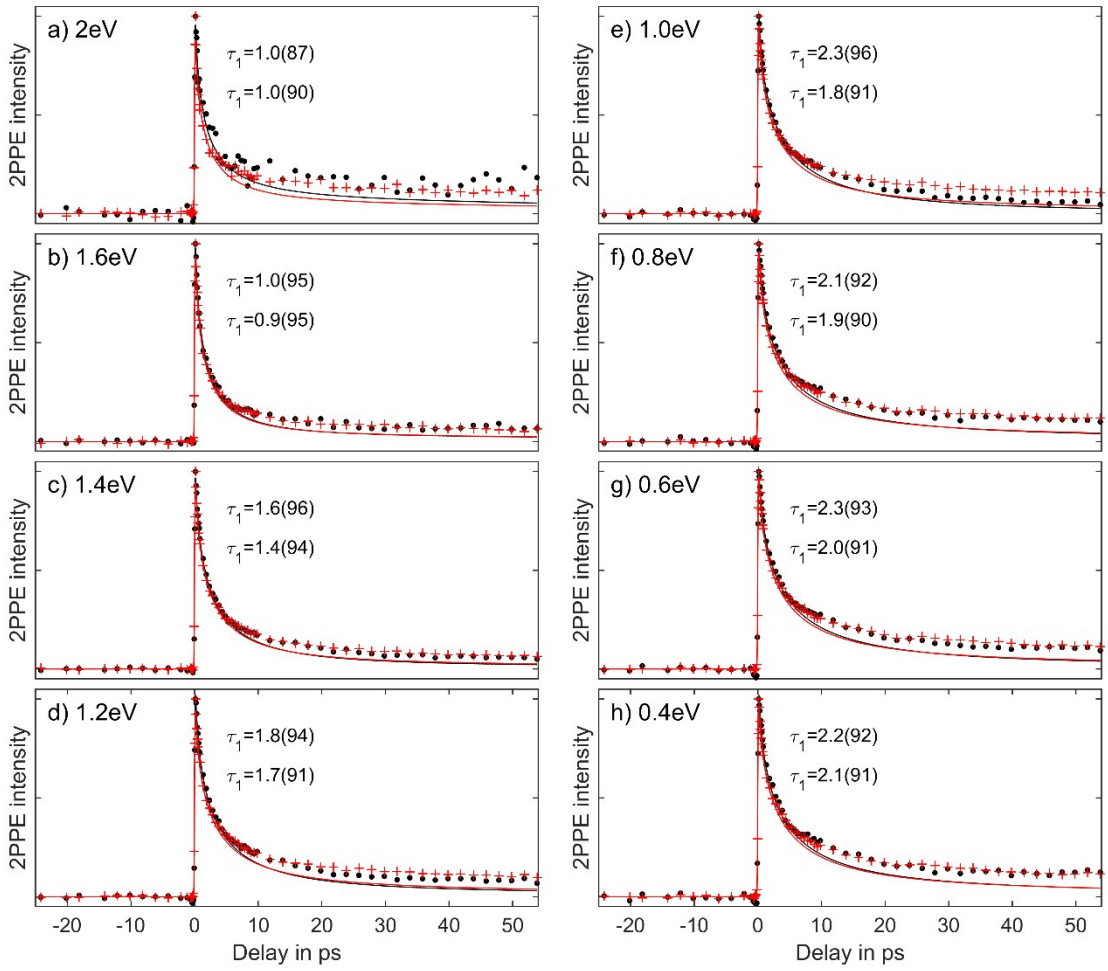

Figure S9. *Time-resolved photoelectron spectroscopy measured with λ_{pump} = 460 nm and λ_{probe} = 257 nm by 2PPE. For a) integration over ΔE_{kin} = 200 meV, for b) - h) over ΔE_{kin} = 100 meV was carried out. Solid lines represent the best fitting approach with a stretched exponential as in equation (10). The numbers in the parenthesis give the relative contributions (A_k) of the lifetimes to the signal in percent. Black circles (•) represent data for as-prepared and red crosses (+) for annealed samples.*

TCSPC fit results and residuals

Below are the residuals for the fits of the TCSPC measurements in Figure S10 and S11 and the fitted values in a Table S2. The relative rms amounts to about maximal 2%.

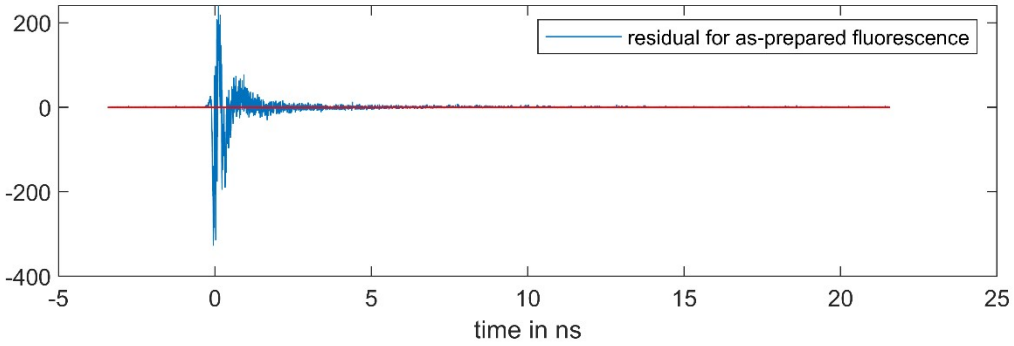

Figure S10. *Residual for TCSPC fit for the as-prepared sample*

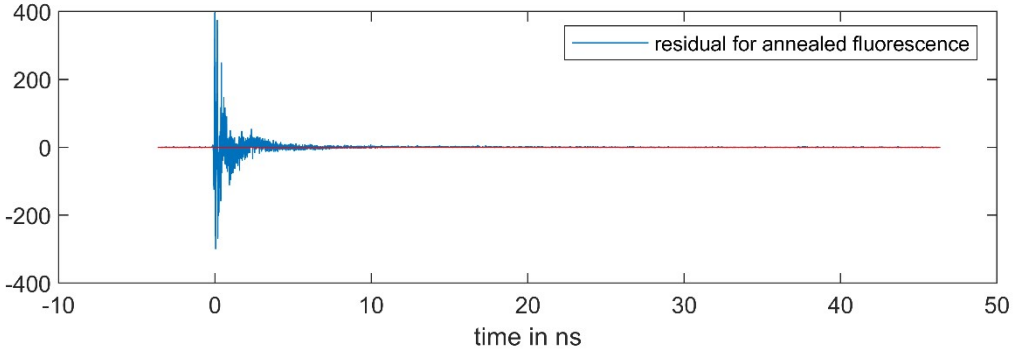

Figure S11. *Residual for TCSPC fit for the annealed sample*

Table S2 *Summarized fit results for the fluorescence lifetimes deduced by TCSPC for as-prepared and annealed pF8T2 thin films on H- terminated silicon*

	as-prepared	annealed
A_1	(87.1 ± 0.1) %	(68.9 ± 0.02) %
A_2	(12.3 ± 0.1) %	(30.1 ± 0.02) %
A_3	(0.55 ± 0.04) %	(1.01 ± 0.01) %
τ_{1F}	(0.15 ± 0.01) ns	(0.14 ± 0.01) ns
τ_{2F}	(0.46 ± 0.01) ns	(0.58 ± 0.01) ns
τ_{3F}	(1.77 ± 0.07) ns	(2.42 ± 0.02) ns

1 P. J. Brown, D. S. Thomas, A. Köhler, J. S. Wilson, J.-S. Kim, C. M. Ramsdale, H. Sirringhaus and R. H. Friend, *Phys. Rev. B*, 2003, **67**, 064203.
2 P. K. H. Ho, J.-S. Kim, N. Tessler and R. H. Friend, *J. Chem. Phys.*, 2001, **115**, 2709–2720.
3 F. C. Spano, *J. Chem. Phys.*, 2005, **122**, 234701.
4 C. Scharsich, R. H. Lohwasser, M. Sommer, U. Asawapirom, U. Scherf, M. Thelakkat, D. Neher and A. Köhler, *J. Polym. Sci. B Polym. Phys.*, 2012, **50**, 442–453.
5 J. Clark, C. Silva, R. H. Friend and F. C. Spano, *Phys. Rev. Lett.*, 2007, **98**, 206406.
6 F. Dou, J. Li, H. Men and X. Zhang, *Polymers*, 2020, **12**, 786.
7 G. Jo, J. Jung and M. Chang, *Polymers*, 2019, **11**, 332.
8 T. Ma, Z. Wang, C. Song, N. Song, J. Ren, B. Liu, H. Zhang, H. Zhang and D. Lu, *J. Phys. Chem. C*, 2019, **123**, 24321–24327.
9 F. C. Spano, *Acc. Chem. Res.*, 2010, **43**, 429–439.